Available online at www.sciencedirect.com

ScienceDirect

Procedia Structural Integrity 3 (2017) 508–516

Structural Integrity Procedia

www.elsevier.com/locate/procedia

XXIV Italian Group of Fracture Conference, 1-3 March 2017, Urbino, Italy

Ductile fracture assessment of X65 steel using damage mechanics

Gabriel Testa[a]*, Nicola Bonora[a], Domenico Gentile[a], Antonio Carlucci[b], Yazid Madi[c]

[a]*Università di Cassino e del Lazio Meridionale, Cassino I-03043, Italy*
[b]*SAIPEM SA, Montigny-le-Bretonneux F-78180, France*
[c]*EPF-Ecole d'ingénieurs / MINES ParisTech, Paris F-75006, France*

Abstract

Strain-based design for offshore pipeline requires a considerable experimental work aimed to determine the material fracture toughness and the effective strain capacity of pipe and welds. Continuum damage mechanics can be used to limit the experimental effort and to perform most of the assessment analysis and evaluation at simulation level. In this work, the possibility to predict accurately ductile rupture in X65 class steel for offshore application, using a CDM model, is shown. The procedure for material and damage model parameters identification is presented and applied to X65, customer grade steel. Then, damage model predictive capabilities have been validated predicting ductile crack growth in SENB and SENT fracture specimen.

Keywords: Ductile fracture; X65 steel; Damage mechanics.

1. Introduction

Pipelines transporting fuel in remote areas can be subjected to deformation well beyond the elastic limit of the material. Under such conditions, strength, toughness and the ability to deform of pipe and weld metal are also decisive for the design. Traditionally, most of pipeline installations worldwide have been designed in accordance to stress-based design principles that pose restrictions in terms of pipe material, property requirements and weld procedure qualification procedures (Yoosef-Ghodsi, 2015). Pipelines in arctic areas are exposed to challenging loading conditions such as permafrost, fault crossings, and ice scouring, which can impose localized high strain. Today, strain based-design is used to guarantee that line pipe sections should be able to deform beyond the elastic range without

* Corresponding author. Tel.: +39.07762993693.
E-mail address: gabriel.testa@unicas.it

10.1016/j.prostr.2017.04.057

failure in consideration of strain demand and available strain capacity. In recent years, both onshore and offshore pipelines have been installed successfully that compensate for strain up to 4% (Mørk, 2007). At present, no fully validated engineering criticality assessment (ECA) exists for strain in excess of 0.5% considering the effect biaxial loading due to internal pressure. Full-scale tests of pressurized pipes at large strain have shown a reduction of the pipeline capacity with a factor of two compared with non-pressurized pipe. This behavior can be ascribed to stress triaxiality effect on material strain capacity that cannot be accounted for by traditional fracture mechanics concepts. Alternatively, continuum damage mechanics (CDM) can be successfully used to predict ductile tearing and rupture in pipeline steels and welds ensuring transferability from laboratory sample to full-scale component (Carlucci et al., 2014a, Carlucci et al., 2014b, Carlucci et al., 2014c).

In this work, the CDM model, as formulated by (Bonora, 1997), was used to predict ductile rupture in API X65, customer grade steel. The approach is based on numerical simulation and dedicated experimental tests. Firstly, the material flow curve and damage model parameters have been identified according to the procedure presented here. Successively, the model predictive capabilities have been validated anticipating material fracture resistance in flawed samples under different loading conditions and comparing with laboratory data. The possibility to implement the proposed procedure in support of strain-based design route is discussed.

2. Ductile damage model

The Bonora Damage Model (BDM) is derived in the framework of continuum damage mechanics where the set of constitutive equations for the damaged material are the same as for the virgin material but the stress is replaced by the "effective" stress (Kachanov, 1958)

$$\tilde{\sigma} = \frac{\sigma}{1-D} \tag{1}$$

D is the damage variable that, under the assumption of isotropic damage, is a scalar. Making the strain equivalence hypothesis – which states that the strain associated with a damage state, under a given applied stress, is equivalent to the strain associated with its undamaged state under the corresponding effective stress – the following definition of damage is obtained,

$$D = 1 - \frac{\tilde{E}}{E_0} \tag{2}$$

According to the second principle of thermodynamics, the mechanical dissipation has to be positive:

$$\sigma_{ij} : \dot{\varepsilon}_{ij}^{p} - Y\dot{D} - A_k \dot{V}_k \geq 0 \tag{3}$$

Here, $\dot{V}_k$ indicates the rate of internal variables, A_k indicates the associated variables, and $-Y$ is the damage (elastic) strain energy release rate defined as,

$$-Y = \frac{\sigma_{eq}^2}{2E\left(1-D\right)^2} R_\nu \tag{4}$$

where

$$R_\nu = \left(2/3\right)\left(1+\nu\right) + 3\left(1-2\nu\right)\left(\sigma_m / \sigma_{eq}\right)^2 \tag{5}$$

is the function that accounts for stress triaxiality defined as the ratio between the mean and the equivalent Von Mises stress. Plastic flow can occur without damage and, similarly, damage can occur without noticeable macroscopic plastic flow. Therefore, it can be assumed that dissipation potential due to the deformation process (and hardening) and the damage process are uncoupled. Then, the overall dissipation potential can be written as,

$$F = f_p\left(\tilde{\sigma}_{ij}, \tilde{A}_k; T\right) + f_D\left(Y; T, D\right) \tag{6}$$

where T is the temperature. From the generalized normality law, the following expression for damage evolution law is obtained,

$$\dot{D} = -\frac{\partial F}{\partial Y} = -\frac{\partial f_D}{\partial Y} \tag{7}$$

The following assumptions differentiate the BDM from other similar formulations.

A) The damage variable D, depends on the "active" plastic strain defined as the equivalent plastic strain accumulated under positive stress triaxiality only:

$$\dot{\hat{p}} = \dot{\varepsilon}_{eq}^{\mathrm{p}} \left\langle \frac{\sigma_m}{\sigma_{eq}} \right\rangle \tag{8}$$

where $\langle ... \rangle$ is the Heaviside function equal to 1 when $\sigma_m / \sigma_{eq} \geq 0$ and 0 otherwise. Under negative stress triaxiality, no damage growth can occur and damage effects are temporarily restored.

B) The following expression of the damage dissipation potential is used,

$$f_D = \left[\frac{1}{2}\left(-\frac{Y}{S_0}\right)^2 \frac{S_0}{1-D}\right]\left[\frac{\left(D_{cr} - D\right)^{\frac{\alpha-1}{\alpha}}}{\left(\hat{p}\right)^{\beta}}\right] \tag{9}$$

here, S_0 is a material constant, α is the damage exponent, $\beta=(2+n)/n$ and n is the hardening exponent. This assumption implies that the damage dissipation depends on the deformation history, which leads to a nonlinear evolution of damage with the active plastic strain.

C) The material flow curve identified in uniaxial tensile test already accounts for damage effects: no softening term is then necessary (Pirondi and Bonora, 2003),

$$f_p = \sigma_{eq} - \sigma_y\left(p\right) \leq 0 \tag{10}$$

This assumption provides the advantage to avoid mesh dependence effect in finite element applications.

From Eqn. (7) and Eqn. (9) together with the definition of Y, and assuming a power law expression for the material flow curve, the following expression for the kinetic law of damage evolution can be obtained,

$$\dot{D} = \alpha \cdot A \cdot R_v \left(D_{cr} - D\right)^{\frac{\alpha-1}{\alpha}} \frac{\dot{\hat{p}}}{\hat{p}} \tag{11}$$

where $A = D_{cr}^{1/\alpha} / \ln\left(\varepsilon_f / \varepsilon_{th}\right)$. More details on the derivation of eqn. (11) can be found in (Bonora, 1997). Under proportional loading condition, Eqn. (11) can be integrated leading to,

$$D = D_{cr}\left\{1-\left[1-\frac{\ln\left(\hat{p}/\,p_{th}\right)}{\ln\left(\varepsilon_f\,/\,\varepsilon_{th}\right)}R_v\right]^{\alpha}\right\} \tag{12}$$

At low stress triaxiality, the threshold strain for damage initiation can be assumed independent of stress triaxiality, then the following expression for the material failure strain $\hat{p}_f$ can be derived,

$$\hat{p}_f = \varepsilon_{th}\left(\frac{\varepsilon_f}{\varepsilon_{th}}\right)^{\frac{1}{R_v}} \tag{13}$$

This expression provides an immediate estimation of the equivalent "active" plastic strain at failure for given stress triaxiality level.

3. Damage model parameters identification

The damage model requires four material parameters to be determined: ε_{th}, which is the uniaxial strain threshold at which the damage processes are initiated, ε_f, is theoretical uniaxial failure strain for $\sigma_m / \sigma_{eq} = 1/3$, D_{cr} is the value of damage at failure and α is the damage exponent.

The identification of damage model parameters can be done according to different methods and experimental techniques (Bonora, 1999, Bonora et al., 2005, Bonora et al., 2008). Stiffness loss measurements with increasing plastic strain are necessary to determine the damage exponent α, while microscopic analysis is required to determine the critical damage at rupture. However, for what concerns the determination of ductile rupture condition under a generic stress triaxiality state of stress, only information on ε_{th} and ε_f are strictly necessary. These two parameters can be determined in two ways. The simplest is to perform uniaxial traction tests on round notched tensile bar (RNB) specimens. From these tests, the failure strain can be determined experimentally from the measure of the minimum section diameter at fracture using the well-known Bridgman expression,

$$\varepsilon_f = 2\ln\left(\frac{\phi_0}{\phi_R}\right) \tag{14}$$

The corresponding stress triaxiality, for each RNB, has to be determined by finite element simulation. It is know that stress triaxiality is not constant along the sample minimum section and it varies during loading. Thus, a reference value can be determined as average of the stress triaxiality at damage initiation and rupture. Finally, these data can be fitted using Eqn. (13) in order to determine ε_{th} and ε_f, respectively. This methodology suffers the fact that both fracture strain and stress triaxiality are defined based on given definitions and a fitting procedure.

Alternatively, damage parameters can be determined using an inverse calibration procedure in which, by means of optimization, both ε_{th} and ε_f are determined minimizing the error between the predicted point of ductile crack initiation, on the applied load vs minimum diameter reduction (or alternatively, axial elongation, and the experimental data. This procedure, although computationally more expensive, does not suffer of the limitations mentioned above and usually provide more robust parameters estimation (Carlucci et al., 2015).

4. Material and experimental tests

The material under investigation is an API X65, customer grade, seamless pipe steel in both as-received and weld conditions, hereafter indicated as "base metal" (BM) and "weld metal" (WM), respectively. The BM was characterized along pipe axial (L) and circumferential (T) directions. Traction tests were performed at different temperatures (RT,

0°, -20° and -40°C), with a nominal strain rate of 10^{-4}/s, using a smooth axisymmetric sample geometry (SB). The specimen geometry used is shown in Fig. 1.

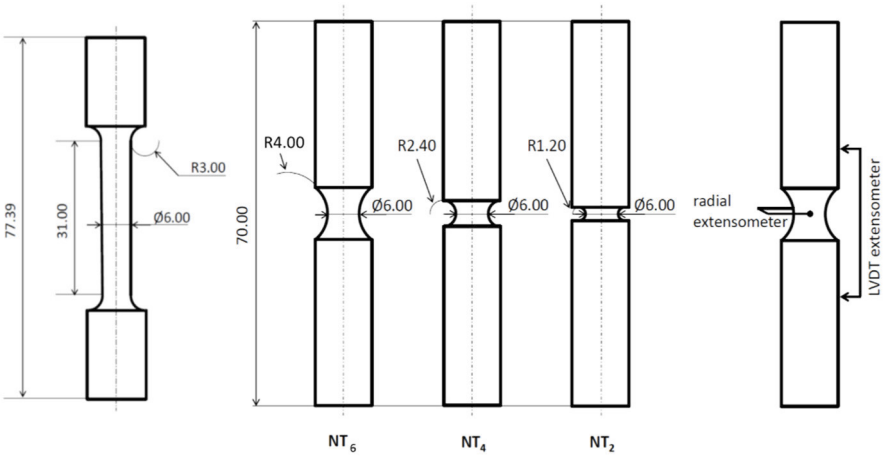

Fig. 1. Uniaxial tensile specimens: smooth round bar (SB) and round notched bars (RNBs). Dimensions in mm.

Uniaxial deformation was measured using a LVDT extensometer with a reference base length of 9.625 mm. Uniaxial traction test results showed a limited variation in the response along the two directions. In Table 1, the summary of average traction tests results at different temperature along T and L direction, are shown. Here, $R_{p0.2}$ is the engineering yield stress at 0.2% strain, R_m is the engineering ultimate stress and ε_r is the strain at rupture calculated with Bridgman expression.

Table 1. Summary of uniaxial tensile properties at different temperatures for X65 BM.

Temperature	Direction	$R_{p0.2}$ [MPa]	R_m [MPa]	ε_r [mm/mm]	$R_{p0.2}/R_m$
RT	L	445.40	548.35	0.135	81.23
	T	446.50	552.25	0.140	80.85
-20°C	L	467.50	594.30	0.110	78.67
	T	462.60	582.30	0.160	79.27
-40°C	L	488.50	610.60	0.160	80.00
	T	468.10	13.00	0.130	75.64

Three different round notch radii have been investigated: 1.2, 2.4 and 4.0 mm respectively. These sample geometries have the same minimum section of the SB (ϕ=6.0 mm) and are identified by the ratio between the notch radius and the minimum diameter: NT_2, NT_4 and NT_6 respectively. Specimen dimensions are shown in Fig. 1.

In the test, the axial deformation and the minimum diameter reduction as a function of the applied load were measured and used for comparison with finite element simulation.

5. Finite element analysis

All finite element simulations were performed using the commercial code MSC MARC v2015. Round samples have been simulated using axi-symmetric, four node element with bilinear shape functions. Elastic-plastic analyses were performed using large displacement, finite strain and Lagrangian updating formulation. The BDM is ready available in MSC MARC and was used for the purpose.

5.1. Base and weld metal flow curve

The identification of the material plastic flow curve was performed as follow. Among all available uniaxial traction test, those in which necking occurred in the gauge length, were selected. Test result, in term of applied load vs extensometer displacement P vs ΔL, was selected as objective function and used in an optimization iterative procedure based on the minimization of the error between available data and FEM calculated response. For the optimization procedure, the mathematical expression for the flow curve needs to be selected. Among all candidate functions, a Voce type law allows to account for the fact that stress have to tend asymptotically to a saturation value for infinite strain. For BM, two terms Voce-type expression was found to be appropriate. However, because the material under investigation shows a considerable Lüders plateau, the following description was used,

$$\sigma = max\left(\sigma_{y0}; A_0 + \sum_{i=0}^{1} R_i\left[1 - exp\left(-\varepsilon_p / b_i\right)\right]\right) \tag{15}$$

where σ_{y0} is the reference yield stress at 0.2% of strain. The hardening in the weld metal was found similar to that of the BM. Therefore, it was decided to assume for the WM the same expression as in eqn. (15) increasing the reference yield stress by the overmatching ratio. The material parameters are summarized in Table 2.

Table 2. Flow curve parameters for BM and WM

	σ_y	A	R_0	R_1	b_1	b_2
BM	450	370.65	146.6	345.94	0.0233	0.384
WM	560	370.65	146.6	345.94	0.0233	0.384

5.2. Damage model parameters

Following the optimization procedure described above, damage parameters have been identified. The critical damage and the damage exponent were assumed the same for both BM and WM.

Table 3. Damage parameters for BM and WM

MATERIAL	ε_{th}	ε_f	D_{cr}	α
BM	0.23	3.5	0.1	0.3
WM	0.10	6.2	0.1	0.3

Files must be in MS Word only and should be formatted for direct printing, using the CRC MS Word provided.

5.3. Model verification

Model verification was performed comparing the predicted specimen, both uniaxial and RNBs, response in terms of applied load vs elongation with experimental data. This comparison provides a first assessment of the material flow curve transferability (from smooth to notched samples) and damage model parameters, at least in the stress triaxiality range typical of these sample geometries.

The comparison is shown in

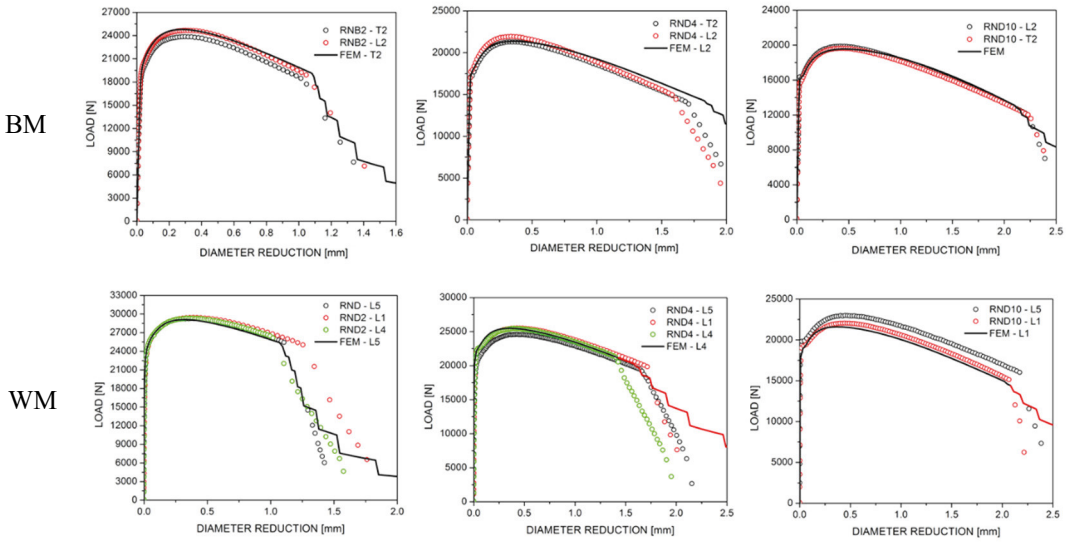

Fig. 2. Comparison of predicted applied load vs elongation response and rupture in RNBs samples for both BM and WM.

5.4. Model validation

Model predictive capabilities were validated predicting global response and crack propagation in SENT and SENB specimens. SENT and SENB with a nominal crack depth/ligament ratio of 0.5 were planned in order to obtain information on the CTOD fracture toughness as prescribed in ECA route. For both geometries, 3D finite element simulations were performed in order to account for loss of constraint occurring under plastic deformation development. Both geometries were modelled using the same mesh along the crack front in order to avoid mesh effects. The minimum element size was 0.2mm x 0.05 mm x 0.05 mm. This element size was determined by means of preliminary parametric investigation performed on NT2 in which the stress triaxiality is close to that occurring in SENB. Crack propagation was simulated using the element removal technique: when damage becomes critical at the Gausspoint, then the element is removed and stresses in the element are released. This feature, which is available in MSC MARC, does not suffer of convergence issues if the load step is relatively small to contain the overall number of elements that fail in the same load increment. No further model parameters adjustment or recalibration was performed at this point.

6. Results

Validation results are shown in the following. In Fig. 3, the comparison of the predicted applied load vs crack mouth opening displacement, and stroke displacement (TRAV), with experimental data for SENT base metal is shown.

The overall agreement is very good and confirmed by the qualitative comparison of the predicted crack growth and crack front shape at test end. It should be noted, that finite element simulation with damage is capable to reproduce all main features of the deformation and growth process included the later contraction which is responsible of the loss of constrain. It is worth to stress that the CTOD for this material at RT is 2.0 mm approximately, which gives an idea of the huge plastic deformation occurring at the crack tip. Because of this, complete failure did not occurred in SENB because the of the complete plastic hinge development.

Similar good agreement was found for SENT. Here, complete ductile failure did occur as shown in Fig. 4. Again, numerical simulation using BDM was able to predict the overall specimen response, the crack growth and later specimen contraction.

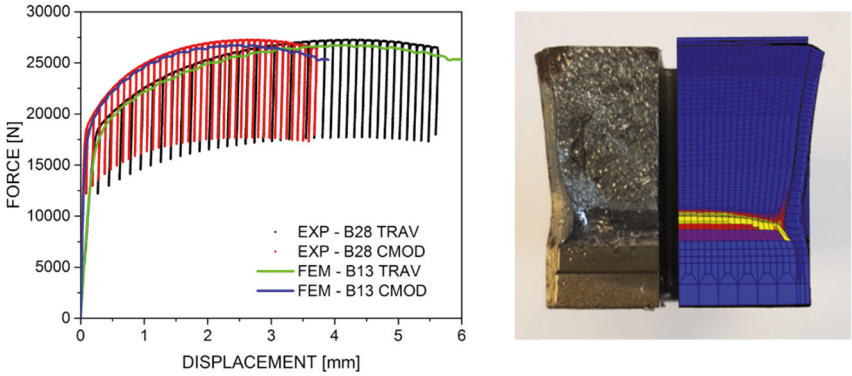

Fig. 3. Comparison of predicted applied load vs displacement (both stroke and CMOD) response and fracture surface for SENB base metal.

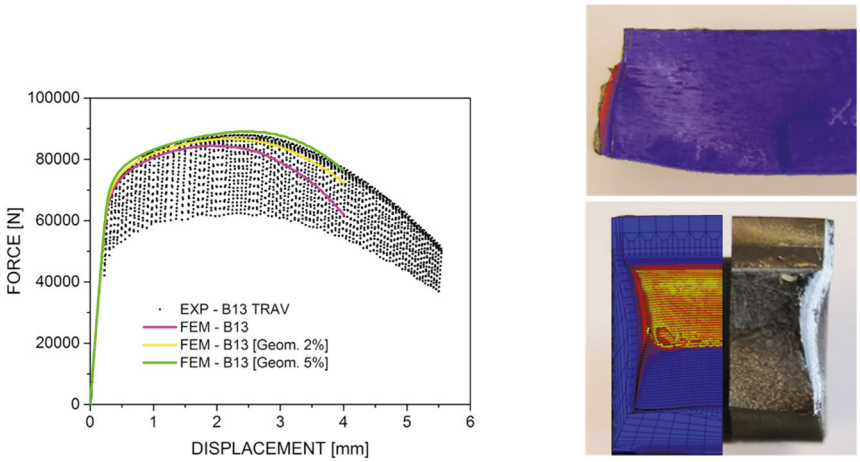

Fig. 4. Comparison of predicted applied load vs displacement (both stroke and CMOD) response and fracture surface for SENT base metal.

Conclusions

In this work, the possibility to predict ductile failure in X65 steel using CDM modelling was shown. The proposed CDM model has a number of features that make it feasible for the use in engineering design route. In particular, the model requires only two parameters that can be easily and objectively determined following a relatively simple procedure. The model parameters identification procedure requires a limited number of simple traction tests that can be inserted in the standard industrial characterization practices. Once calibrated, model parameters are transferable to other sample geometries without the need to perform additional recalibration. From the computational point of view, the time required for a complete rupture simulation in 3D sample (several hundred thousands of brick elements) is of the order of few hours, which is compatible with design process requirement and suitable for simulation of full-scale components.

References

Bonora, N., 1997. A nonlinear CDM model for ductile failure. Engineering Fracture Mechanics, 58, 11-28.
Bonora, N., 1999. Identification and measurement of ductile damage parameters. Journal of Strain Analysis for Engineering Design, 34, 463-478.
Bonora, N., Gentile, D., Pirondi, A., Newaz, G., 2005. Ductile damage evolution under triaxial state of stress: Theory and experiments. International

Journal of Plasticity, 21, 981-1007.

Bonora, N., Ruggiero, A., De Meo, S., Gentile, D., Esposito, L., 2008. A revised approach to damage measurement based on stiffness loss technique. American Society of Mechanical Engineers, Pressure Vessels and Piping Division (Publication) PVP, 195-199.

Carlucci, A., Bonora, N., Ruggiero, A., Iannitti, G., 2015. Procedure to establish critical threshold strain value for strain-based-design in fracture mechanics assessment for ductile material. Proceedings of the International Offshore and Polar Engineering Conference, 646-656.

Carlucci, A., Bonora, N., Ruggiero, A., Iannitti, G., Gentile, D., 2014a. Crack initiation and growth in bimetallic girth welds. Proceedings of the International Conference on Offshore Mechanics and Arctic Engineering - OMAE.

Carlucci, A., Bonora, N., Ruggiero, A., Iannitti, G., Testa, G., 2014b. Crack initiation and propagation of clad pipe girth weld flaws. American Society of Mechanical Engineers, Pressure Vessels and Piping Division (Publication) PVP.

Carlucci, A., Bonora, N., Ruggiero, A., Iannitti, G., Testa, G., 2014c. Integrity assessment of clad pipe girth welds. Proceedings of the International Conference on Offshore Mechanics and Arctic Engineering - OMAE.

Kachanov, L. M., 1958. On Creep Rupture Time. Izv. Acad.Nauk. SSSR, Otd.Techn. Nauk, 8.

Mørk, K., 2007. The Challenges Facing Arctic Pipelines, Design Principles for Extreme Conditions. Offshore Oil and Gas Magazine, 67, 150-151.

Pirondi, A. & Bonora, N., 2003. Modeling ductile damage under fully reversed cycling. Computational Materials Science, 26, pp. 129-141.

Yoosef-Ghodsi, N., 2015. Strain-Based Design of Pipelines. *In:* Revie, R. W. (ed.) *Oil and Gas Pipelines.* John Wiley & Sons, Inc.